PdNi thin films for hydrogen oxidation reaction and oxygen reduction reaction in alkaline media

Electrochimica Acta 420 (2022) 140425

Contents lists available at ScienceDirect

Electrochimica Acta

journal homepage: www.journals.elsevier.com/electrochimica-acta

PdNi thin films for hydrogen oxidation reaction and oxygen reduction reaction in alkaline media

Gerard Montserrat-Sisó *, Björn Wickman

Division of Chemical Physics, Department of Physics, Chalmers University of Technology, Gothenburg SE-412 96, Sweden

ARTICLE INFO

Keywords:
Alkaline Fuel Cells
Hydrogen oxidation reaction
Oxygen reduction reaction
Thin films
PdNi
Palladium
Nickel

ABSTRACT

Pd-based catalysts are considered to be among the most promising electrocatalysts for both the hydrogen oxidation reaction (HOR) and oxygen reduction reaction (ORR) in alkaline media. Although major progress in finding effective catalysts has been made, the reasons for the activity enhancement in alkaline conditions remain to be elucidated. Herein, we report the fabrication of alloyed PdNi thin films as a tool to study the HOR and ORR reactions. Annealing of physically evaporated PdNi thin films at different temperatures results in different surface compositions and a range of HOR and ORR activities in 0.1 M KOH. Moreover, annealed samples were acid treated to remove the surface Ni and the HOR and ORR were investigated to elucidate the effect of surface and subsurface Ni. For the HOR, it was found that the addition of Ni decreases the hydrogen binding energy (HBE) of Pd through an electronic effect, which results in an increase in activity. In addition, it was found that the HOR activity was further increased by the bifunctional effect induced by surface Ni, which provides OH^- adsorption sites. In contrast to HOR, it was concluded that surface Ni was disadvantageous for the ORR. However, subsurface Ni was found to induce an electronic effect on Pd that resulted in a somewhat improvement of the ORR kinetics by improving its oxygen desorption. These results provide insights for more tailored design of electrocatalysts in alkaline media by shedding new light on the mechanisms through which the HOR and ORR kinetics are improved in alkaline media.

1. Introduction

Low-temperature fuel cells have been recognized during the last decades as promising power generation technologies for both stationary and portable applications. Because of their high energy density, small size, and lightweight, Proton Exchange Membrane Fuel Cells (PEMFC) have become the current leading low-temperature fuel cell for automotive applications [1,2]. However, the widespread commercialization of PEMFC in automotive vehicles is currently impeded by their high cost and limited lifetime. Both limitations are greatly attributed to the catalyst layer, whose contribution to the total cost of the fuel cell stack for large-scale energy production is nearly half [3,4]. This high cost is to a large degree due to the scarcity of platinum, of which high amounts are needed to catalyze the hydrogen oxidation reaction (HOR) in the anode and to improve the sluggish oxygen reduction reaction (ORR) kinetics in the cathode [5,6]. Thus, Pt-based catalysts have limited availability and the activity in acidic media is not sufficient to meet the efficiency target [7]. In contrast to acidic media, the rather mild alkaline conditions in the Anion Exchange Membrane Fuel Cell (AEMFC) allow the use of Pt-free electrocatalysts, which brings up new possibilities of finding abundant and inexpensive electrocatalysts without compromising the power density of the fuel cell [8,9]. A high pH environment implies different electrode reaction mechanisms. The kinetics of the ORR in alkaline media is more facile than in acid [10] and the overpotential for the ORR is lowered at high pH environments, which allows the use of non-Pt metals [11]. Despite the activity enhancement in alkaline media, the ORR activity is still far from being optimal and affordable catalyst with high activity and stability are yet to be developed.

Similar to that in acidic media, an ideal catalyst for the ORR in alkaline media should have an adsorption energy of hydroxides about 0.1 eV lower than that of Pt(111) [12]. One strategy to modify the OH^- adsorption is through alloying with metals with different d-orbital occupancies. It has been reported that through changes in the d-orbital overlap that change the d-band center, the breakage of the O–O bond, as well as the desorption of oxygenated intermediates, can be tuned [13]. By coupling a metal with low occupancy of d-orbitals with another high occupancy d-orbital metal, the d-band center of the fully occupied d-orbital metal is lowered, resulting in an ORR enhancement for

* Corresponding author.
E-mail address: gerard.siso@chalmers.se (G. Montserrat-Sisó).

https://doi.org/10.1016/j.electacta.2022.140425
Received 29 September 2021; Received in revised form 21 April 2022; Accepted 21 April 2022
Available online 23 April 2022

platinum group metals (PGMs) [15]. This enhancement is caused by the significant decrease in the Gibbs free energy of key electron transfer steps, which results in an optimal balance between the O_2 bond breaking and the adsorption of oxygenated species [14,15]. Thus, this electronic effect induced in PGMs with alloying plays a crucial role in the enhancement of the ORR activity of PGMs in both alkaline and acidic conditions.

In contrast to the ORR, the HOR kinetics at the anode is greatly hindered in alkaline conditions compared to acidic [16]. The anodic reaction on Pt under alkaline conditions is around two orders of magnitude slower than that in acid [17,18]. Although the HOR mechanism in alkaline media is not fully understood, it is considered to proceed through either the Tafel-Volmer or Heyrovsky-Volmer mechanism:

$$(Tafel)\ H_2 + 2^* \rightarrow 2H_{ad} \quad (1)$$

$$(Heyrovsky)\ H_2 + OH^- + * \rightarrow H_{ad} + H_2O + e^- \quad (2)$$

$$(Volmer)\ H_{ad} + OH^- \rightarrow H_2O + e^- + * \quad (3)$$

Regardless of the mechanism, it is known that one reason behind the much slower HOR mechanism is the adsorption of oxygenated species blocking H_2 adsorption sites [19]. However, the hydrogen binding energy (HBE) is considered to be a highly important factor controlling the HOR kinetics. The reason for this is that the initial dissociative adsorption of hydrogen is likely to be the rate determining step, also in the presence of oxygenated species [9,20,21]. Hence, previous studies suggest that finding catalysts with both oxophilic sites that bond OH^- groups reversibly and sites with an optimal HBE, combining in a so-called bifunctional surface, is crucial to boost the HOR kinetics at the anode [22–25]. However, other studies also claim that the HBE is the sole and unique descriptor for the HOR in the full range of solution pHs and that the HBE should be decreased if the HOR activity is meant to be improved [16,26–28]. This lack of agreement on which is (or are) the critical factors governing the HOR activity in alkaline media hinders the design of new HOR electrocatalysts.

Palladium has been intensively investigated as a potential candidate to substitute Pt in high pH environments and several reviews of Pd-based catalysts have been published to date [29–31]. Pd represents a good alloying material for ORR due to its fully occupied d-orbitals that could promote the electronic effect, as well as for HOR because of its close to optimal HBE [32]. To improve both anodic and cathodic kinetics, Pd needs to be alloyed with a metal with low d-orbital occupancy to optimize the oxygen adsorption for ORR and enough oxophilicity to promote the adsorption of hydroxide and avoid the blockage of Pd sites for hydrogen adsorption in HOR. Nickel is a very inexpensive and abundant metal that fulfills both requirements. Thus, a catalyst containing both Pd and Ni could potentially exhibit promising electrocatalytic activity for both reactions [33–37].

It has been suggested that both bifunctional and electronic effects play a crucial role in enhancing the electrocatalytic activity of PdNi catalysts. The mechanism through which the HOR activity is enhanced in alkaline media when alloying Pd with Ni is not completely understood. The role of Ni in boosting the HOR kinetics is believed to occur either by providing oxophilic sites for the adsorption of hydroxyl species (bifunctional effect) or by affecting the HBE (electronic effect) [38–40]. It has been found that the HOR activity is dependent on the coverage of Ni oxidated species because of their higher oxophilicity when compared to metallic Ni [41,42]. Thus, bifunctional effects need the correct surface distribution of Pd and Ni oxidated species if the rate enhancement is meant to be observed, with OH^- binding on Ni and hydrogen binding on adjacent Pd [24,33]. For ORR, instead, the electronic effects require Pd to be in contact with oxygenated species and Ni in the contiguous subsurface for the correct bimetallic synergy and thus an improvement of the oxygen adsorption on the Pd surface [35]. With the aim to corroborate the mechanisms of bifunctionality for HOR and bimetallic coupling for ORR, PdNi alloys [33,34], core-shells [24], nanocrystals [43] and PdNi nanoparticles [44–46] have been investigated in the literature. However, there are still many questions regarding the mechanisms through which the enhancement takes place in both reactions, whose exploration is hindered by the lack of knowledge about the elementary steps. For HOR it is often claimed that the HBE is the only descriptor affecting the alkaline activity [47], while other investigations suggest that the adsorption of OH also influences the activity, albeit to a lesser extent [25]. Thus, the role of adsorbed H and OH is crucial to completely understand the HOR mechanism in alkaline media [48]. For the ORR, the discussion arises from the mechanisms through which the intermediate species promote the desired 4-electron pathway rather than the 2-electron pathway [49,50]. Thin films present the advantage of being well defined, making the fabrication of different alloy stoichiometries more facile due to the high control over composition. They also have large surface areas with minimized loadings compared to their polycrystalline analogs and they are straightforward to characterize, which means they offer a good platform for mechanistic studies.

This study presents a comprehensive electrochemical and compositional characterization of PdNi annealed thin film alloys linked with their catalytic activity for both HOR and ORR reactions in 0.1 M KOH. Thin films present the advantage of being well defined, making the fabrication of different alloy stoichiometries more facile due to the high control over composition. They also have large surface areas with minimized loadings compared to their polycrystalline analogs and they are straightforward to characterize, which means they offer a good platform for mechanistic studies. Physically evaporated thin films are thus annealed at different temperatures and the differences in HOR and ORR electrocatalytic activities are discussed for different XPS surface compositions. The results suggest that, although HBE is the main descriptor, the presence of surface Ni is still favorable for the HOR activity, while the ORR is impeded by Ni present on the surface. Instead, the ORR activity can be improved by an electronic effect if Ni is situated beneath the Pd.

2. Experimental

2.1. Fabrication and annealing of PdNi thin films

Fabrication of thin films was carried out in cleanroom facilities of Fed. Std.209E Class 10–100. Electron-beam evaporation (PVD 225 from Lesker) was used to evaporate PdNi thin films on glassy carbon substrates (5 mm diameter diamond polished Sigradur G disks from HTW Gmbh). The carbon disks were first cleaned by sonication in acetone, isopropanol, and Milli-Q water for 10 min in each solvent followed by plasma cleaning with O_2 at 150 W (Plasma-Therm). In order to avoid oxidation of Ni in air, 12 nm of Ni was first evaporated on the carbon substrate followed by evaporation of 28 nm of Pd, resulting in a 40 nm thin film with an atomic ratio of 1:1 and loadings of 14.4 $\mu g_{Pd}/cm^2$ and 24.9 $\mu g_{Ni}/cm^2$. In order to induce alloy formation, the samples were subsequently annealed at different temperatures in a flow reactor for 48 h in 4% H_2 in Ar carrier gas at a flow rate of 500 mL min^{-1} to avoid oxidation (Fig. S1, Supporting Information). Annealed samples were additionally acid treated with 0.1 M HCl for 10 min with the aim of forming a protective Pd overlayer by removing Ni oxide on the surface. Below, we shall refer to the samples as PdNi-X for annealed samples (where "X" represents the annealing temperature) and PdNi-X-AT for acid treated samples annealed at the same temperature.

2.2. Electrochemical measurements

A three-electrode rotating disk electrode (RDE) cell was used to perform all the electrochemical measurements. The RDE cell (Pine Instruments) was equipped with a graphite rod (Sigma-Aldrich, 150 mm length and 3 mm diameter) as a counter electrode (CE). Graphite was chosen as CE to avoid metal contamination of the working electrode

(WE), a very likely event in alkaline electrolytes [51–53]. A PTFE HydroFlex® Hydrogen Reference Electrode (Gaskatel) was used as a reference electrode (RE) and all the potentials in this study refer to that of the RHE. The reliability of the RHE potential was continuously tested experimentally by bubbling H_2 over a Pt WE in the same electrolyte and measuring the intersection of zero current by cycling the potential between −0.02 V to 0.02 V vs RHE at 2 mV/s. The setup was also equipped with a gas inlet on the side of the cell to allow the electrolyte to be saturated with gasses. The potentiostat used (SP-300 from Bio-Logic®) was controlled with the EC-lab software. The samples were mounted on an RDE PTFE tip from Pine Instruments using PTFE U-cups. Although the recommended practice is using a PTFE cell for alkaline electrolytes [21], a glass cell was used for the RDE measurements due to the short period and rather mild alkaline conditions of the measurements.

The electrochemical cell and the glassware were cleaned prior to the measurements in piranha solution (98% H_2SO_4 (Sigma-Aldrich, Emsure) and 33% H_2O_2 (VWR Chemicals, Technical), 3:1 v/v) for at least 24 h. The cell was then thoroughly rinsed with ultrapure water (18.2 MΩ cm, <3 ppb TOC, Milli-Q® IQ 7000, Merck) at least 10 times before each measurement. The electrolyte used for ORR and HOR measurements consisted of 0.1 M KOH prepared from KOH pellets (KOH hydrate ≥99.995%, Suprapur®, Merck) and ultrapure water. The electrolyte was prepared and stored in a PFA volumetric flask (BRAND®) to prevent contamination over time from glass corrosion [54]. A 0.1 M HCl solution prepared from 30% HCl (Suprapur®, Merck) was used for the acid treatment of the samples. The Ar used for de-oxygenation of the electrolyte was supplied by AGA with instrument 6.0 purity, O_2 by Strandmøllen (≥ 99,6 vol%) and H_2 by Air Liquide (≥ 99,999 mol%).

In order to measure on a stable surface free of impurities, a conditioning scheme was conducted for every sample before every measurement. Conditioning was conducted under inert atmosphere after Ar purging, no rotation and consisted of 150 cycles between 0.1 and 1.2 V vs RHE at 150 mV/s. Cyclic voltammetry between 0.05 and 1.35 V vs RHE at 50 mV/s until stabilization of the voltammogram was recorded after conditioning. After CV, the electrolyte was saturated with either H_2 or O_2 and HOR/ORR polarization curves were measured at 50 mV/s at different electrode rotation speeds varied between 400 and 2500 rpm. We chose this scan rate due to contamination issues, which are more severe at low scan rates in liquid electrolyte [55]. The electrolyte was then Ar-saturated and another CV under the same conditions was recorded to evaluate changes of the surface from HOR/ORR. All potentials were corrected for ohmic losses by iR-compensation. The Ohmic resistance was determined by electrochemical impedance spectroscopy (EIS) from the intercept in the Nyquist plot [56]. The intersection of the imaginary impedance between 10 and 20,000 Hz on the real impedance was used to calculate the uncompensated resistance of the solution, which depends on the ionic conductivity of the electrolyte and geometry of the cell [57]. The typical measured resistance in 0.1 M KOH ranged from 40 to 50 Ω and was measured prior to each experiment in Ar-saturated electrolyte with no rotation. The iR-compensation was applied after obtaining the I-V polarization curve.

2.3. Physical characterization

Scanning electron microscopy (SEM) was used to image the annealed samples. SEM was performed using a Zeiss Supra 60VP field-emission microscope with an in-lens detector at 5 kV acceleration voltage and a working distance around 3 mm.

A PHI 5000 VersaProbe III Microprobe X-ray Photoelectron Spectroscopy (XPS) instrument (Physical Electronics) was used to study the surface composition of the thin films. The instrument is equipped with a monochromatic Al K-α X-Ray excitation source (1486.6 eV) operated at 50 W as well as a dual charge compensation: an electron neutralizer (negative charge compensation) and an ion gun (positive charge compensation). Surface composition was evaluated by a survey scan in the binding energy range between 0 and 1400 eV with an energy step width of 0.4 eV. The chemical states of Pd-3d, Ni-2p, C-1 s and O-1 s core level spectra were studied in the narrow scan, which were recorded with an energy step of 0.1 eV and a pass energy of 55 eV. The measuring area was about 200 μm in diameter. The chamber pressure was always lower than 5.0×10^{-9} mbar during measurements. XPS measurements were performed for annealed samples, after dipping in 0.1 M HCl and after RDE testing. For all samples, the binding energy scale was corrected by shifting the spectra with respect to the adventitious C-1 s peak of the C–C bond to 284.8 eV. Depth profiling was used in the same XPS instrument to map the elemental composition throughout the thin films and detect a potential thickness loss after RDE measurement. It was carried out by successive 2 kV Ar^+ ion etchings over a 2×2 mm^2 area at a rate of 4 nm/min. Both survey and narrow scans were recorded every 5 nm throughout a 40 nm depth. For the layer analysis narrow scans were recorded with 69 eV pass energy and 0.2 eV/step.

Relative sensitivity factors from the PHI-Multipak software were used for the concentration quantification. Concentrations were determined with the effective peak areas after Shirley background subtraction. For the electronic structure and chemical state analysis, the core level spectra of Ni-2p and Pd-3d were curve-fitted with the Multipak software. The fitting routine of the peaks was performed using an asymmetric Gaussian-Lorentzian sum function with a Shirley background.

3. Results & discussion

3.1. Characterization of annealed and acid treated PdNi thin films

Physically evaporated PdNi thin films were thermally annealed in 4% H_2 in Ar at temperatures between 350 and 600 °C. Different Pd:Ni surface and subsurface atomic compositions were obtained as a result of different diffusion behaviors at different annealing temperatures. Fig. 1 shows the Pd:Ni atomic concentrations throughout the annealed thin films investigated by ion etching depth profiling in XPS. The depth profile shows the effect of annealing temperature on both surface and subsurface Pd:Ni concentrations. The as-prepared samples were fabricated with a 28 nm Pd film evaporated on top of a 12 nm Ni film to achieve 1:1 atomic ratio of Pd and Ni. The sample annealed at 350 °C shows a Pd:Ni composition at the surface of about 60% Pd (40% Ni), which indicates that Ni diffuses through the Pd film and reach the surface already at this temperature. The PdNi-350 profile shows that the Ni content decreases when going from 0 to 5 nm depth, indicating the

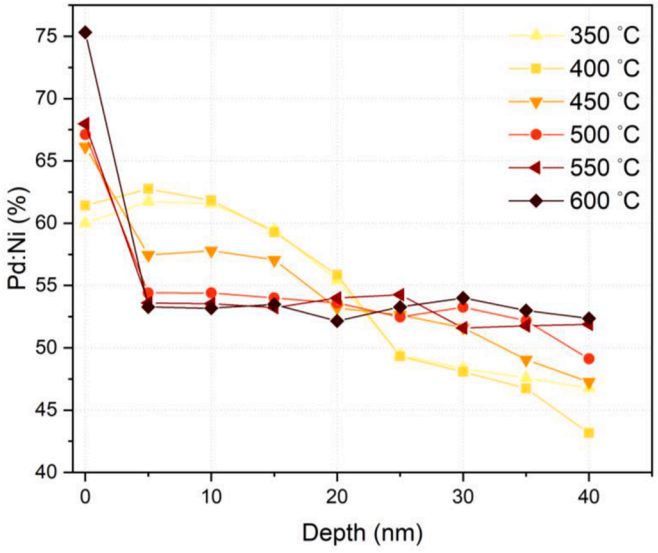

Fig. 1. Pd:Ni composition profile of thin films at different annealing temperatures obtained from Ar^+ ion etching depth profile in XPS.

preference of Ni to be at the surface at 350 °C. After depths of 10 nm, the amount of Pd gradually decreases. At 40 nm depth the amount of Pd is over 40%, confirming that at this temperature Pd and/or Ni mobility is already sufficient to diffuse throughout the entire film. At 400 °C a similar behavior is observed, with Ni accumulating on the surface rather than in subsurface layers and increasing concentration throughout the sample depth. This lower Ni content in the subsurface can be explained by the preferential sputtering event towards the lighter element in XPS depth profiling due to their larger cross-section, which renders a slight overestimation of the concentration of the heavier element [58] (Figs. S2 and S3, Supporting Information).

Higher annealing temperatures resulted in similar concentration profiles. After annealing at 450 °C and above, Pd:Ni subsurface stoichiometries close to 1:1 were achieved from 5 nm throughout the film. From 450 °C, the amount of Pd on the surface significantly increased and further Pd enrichment on the surface was limited after annealing from 450 to 550 °C. The attained surface ratio of Pd and Ni is explained by their difference in surface energy [59]. At 600 °C there is an abrupt increase of surface Pd to 75% while subsurface concentrations remain unchanged.

The effect of temperature on the grain size of annealed samples is evidenced by SEM images (Fig. 2). As shown in the insets, the grains increase with increasing annealing temperature. The grain size ranged with a large variation from about 20 nm (PdNi-350) to about 200 nm (PdNi-600).

Cyclic voltammograms (CVs) of Pd, Ni, PdNi-400, and PdNi-400-AT in Ar-saturated 0.1 M KOH solution are shown in Fig. 3a. Pure Pd and Ni samples were also annealed at 400 °C to relax the surface and enable better comparison. As can be seen, the annealed alloy (PdNi-400) shows a CV that differs from that of pure Pd and pure Ni. Firstly, although only Pd is active for hydrogen adsorption, the annealed PdNi alloy exhibits a larger hydrogen adsorption/desorption region (between 0.05 and 0.4 V vs. RHE). Possible reasons for this are either the alloying effect, which leads to an increase in lattice spacing and hence may facilitate the hydrogen absorption into the metal lattice [60]; or the overlapping of Ni (II) reduction currents with hydrogen adsorption [61]. Secondly, the peaks emerging at 0.7 – 0.8 V exhibit different intensities and shapes for PdNi and pure Pd. This peak corresponds to the chemisorption of OH^- ions on Pd, followed by plateau-shaped currents ascribed to the oxidation of Pd-OH to higher valence Pd oxides (both PdO and $Pd(OH)_2$) [62,63]. This plateau also comprises currents attributed to the formation of a β-$Ni(OH)_2$ layer [61,64]. The formation of other Ni(II) species is not displayed in the CV due to a potential window not wide enough to entail the potential at which these processes occur [65]. Although the surface of PdNi-400-AT is composed solely of Pd, it does not present the OH^- adsorption peak. The reduction peak at 0.7 V is attributed to the reduction of Pd(II) compounds during the cathodic sweep [61–63]. As seen, the Pd(II) reduction takes place at slightly different potentials for pure Pd, PdNi-400 and PdNi-400-AT. As expected, PdNi-400 shows a lower amount of charge involved on the Pd(II) reduction, indicating less amount of surface Pd. Upon acid treatment, the reduction peak increase in intensity due to the removal of Ni species from the surface, forming a completely Pd covered surface. The reduction peak for PdNi-400-AT is shifted negatively with respect to pure Pd. This suggests that the Pd on the surface of the PdNi-400-AT is affected by the Ni in the alloy below the surface.

Fig. 3b shows both the Pd:Ni XPS atomic concentration and Pd electrochemical active surface area (ECSA) before and after the acid treatment. Since the hydrogen adsorption is accompanied by the absorption of hydrogen into the palladium bulk, ECSA of Pd alloys cannot be readily calculated from the hydrogen underpotential deposition region (H_{UPD}) [66,67]. Instead, we chose to derive the Pd surface area from the charge corresponding to surface oxide reduction region. Hence, the Pd ECSA was calculated by measuring the charge involved in the surface PdO reduction from the peak at 0.7 V vs. RHE and dividing it by the charge density associated to the reduction of a PdO monolayer (424 $\mu C/cm^2$) [68,69]. As seen in Fig. 1, Pd atomic concentration on the top layers of the films increased with increasing annealing temperature, ranging from 60 to 75%. After HCl cleaning for 10 min, all samples exhibited an increase of surface Pd regardless of the Pd:Ni atomic concentration prior to the acid treatment. Pd atomic concentration increased to about 80% of the total surface composition. Pd ECSA, instead, is not dependent on the annealing temperature and it exhibits its maximum at 450 °C (Fig. 3b). The Pd ECSA increase between 350 and 450 °C can be confidently assigned to a surface Pd enrichment. Nevertheless, it must be mentioned that surface roughness decreases with increasing temperature, making the decrease of the Pd ECSA after 450 °C attributable to a smoothening of the total surface area. This is evidenced on the Pd ECSA of the acid treated samples. Since HCl effectively removes oxidated Ni species, it is assumed that the surfaces of all acid treated samples are entirely composed of Pd. Hence, the decrease of Pd ECSA with increasing temperature in the acid treated

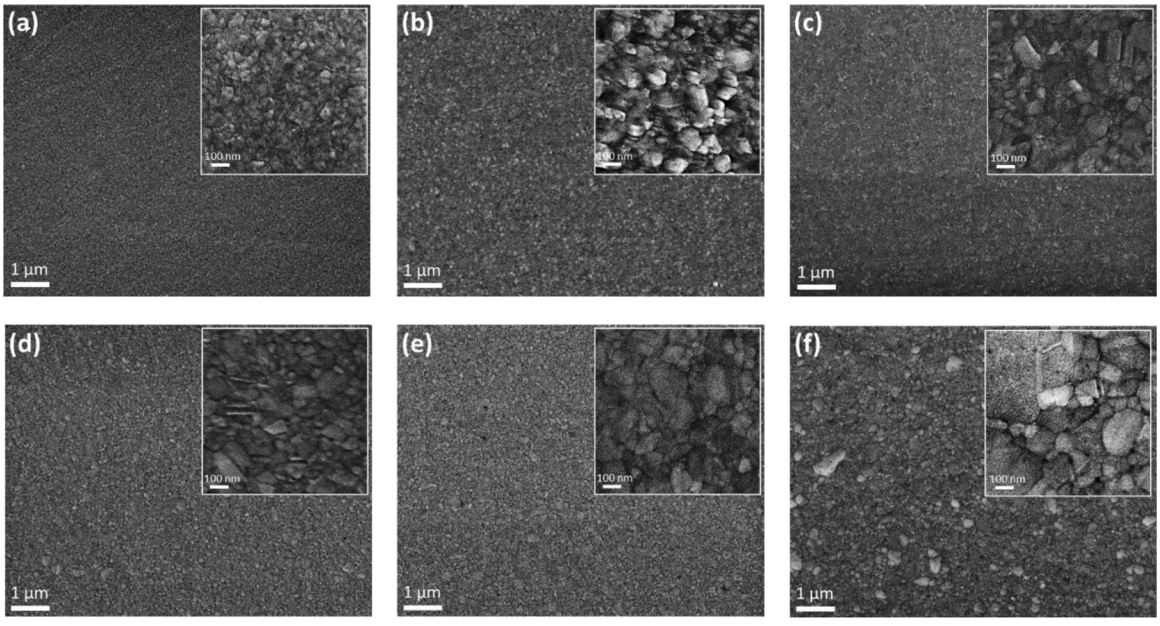

Fig. 2. SEM images of samples annealed at (a) 350 °C; (b) 400 °C; (c) 450 °C; (d) 500 °C; (e) 550 °C and (f) 600 °C.

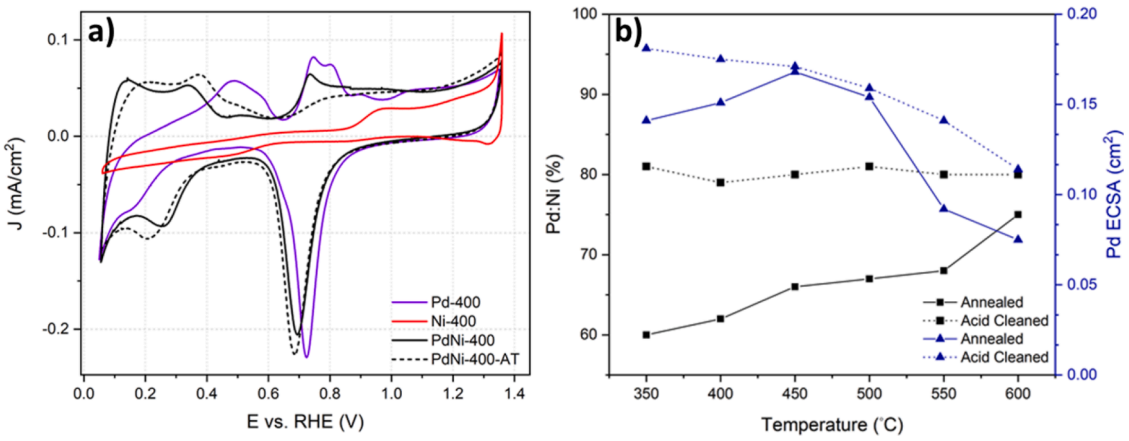

Fig. 3. (a) Cyclic voltammograms in Ar-saturated 0.1 M KOH of Pd, Ni, PdNi annealed at 400 °C and acid treated 40 nm thin films. Scan rate 50 mV/s; room temperature; b) Pd:Ni surface concentrations from XPS and Pd ECSA of annealed samples before and after the acid treatment.

samples is ascribed to a decrease of the total surface area. In this way, it is easily observable that increasing temperature above 500 °C results in a Pd withdrawal from the surface as evidenced by the more pronounced decay of Pd ECSA for the annealed samples. Surface atomic distributions can be inferred by comparing surface compositions obtained in XPS with Pd ECSA profiles. For annealed samples, Pd concentration in both surface layers and on the total surface area increases proportionally until 450 °C, indicating similar atomic distributions in both regions. After 450 °C, the amount of Pd in the outermost layers keeps increasing while Pd ECSA decreases significantly after 500 °C. This trend indicates the formation of a Ni-rich surface with a Pd-rich subsurface at high annealing temperatures. For the acid treated samples, the amount of surface Pd remains constant and the decrease in Pd ECSA is merely attributed to smoothening of the surface with thermal annealing. X-ray diffraction (XRD) analysis was also performed on pure Pd, pure Ni, PdNi as-evaporated and PdNi-X samples (Fig. S6, Supporting Information), which revealed that the Pd(111) diffraction peak is shifting upon annealing and thus confirmed the actual mixing of the two elements.

The surface elemental composition and the chemical state of both Pd and Ni were investigated by XPS on both annealed and acid treated

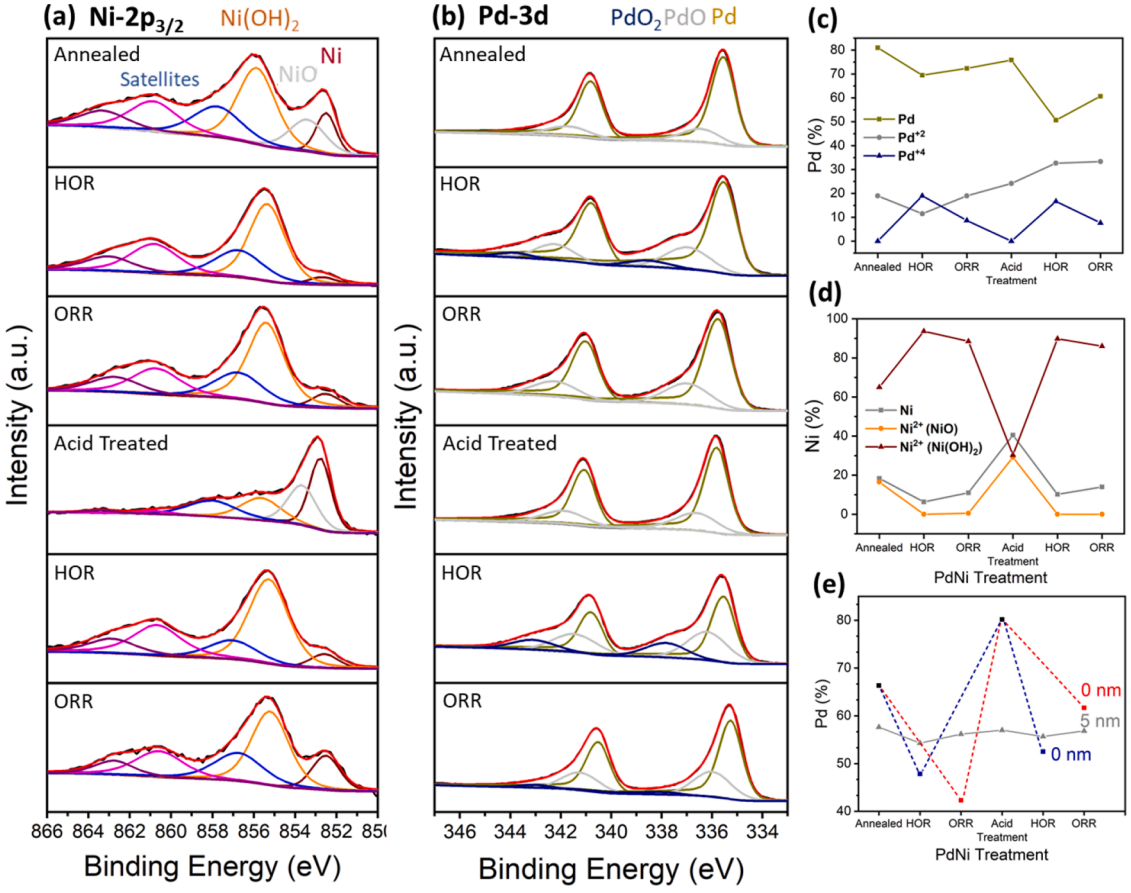

Fig. 4. XPS deconvoluted spectra of (a) Ni-$2p_{3/2}$ and (b) Pd-3d for PdNi-450 and PdNi-450-AT samples; (c) averaged Pd:Ni composition and content of (d) Ni species and (e) Pd species extracted from XPS before and after annealing, acid treatment and electrochemical tests. Dashed lines indicate the change in Pd% upon treatment. Relative percentages of the different Pd and Ni species as well as Pd:Ni composition average are shown in Table S2 (Supporting Information).

samples, as well as after the electrochemical tests. For the Ni-2p XPS spectra, only the $2p_{3/2}$ splitting was deconvoluted (Fig. 4a) and the sensitivity factor corresponding to one peak doublet was used for quantification. Three binding energies of three Ni species were distinguished in the core level spectra: Ni ($2p_{3/2}$: 852.6 eV); Ni^{2+} in NiO ($2p_{3/2}$: 853.7 eV); and Ni^{2+}in $Ni(OH)_2$ ($2p_{3/2}$: 855.6 eV) [70–72]. Gaussian-Lorentzian peaks were used for the deconvolution of all Ni species and Pd oxides, whereas metallic Pd peaks were fitted using asymmetric peaks. An iterated Shirley background was subtracted from all data and all Ni and Pd deconvoluted peaks were allowed to vary by ±0.3 eV.

The relative content of Pd and Ni species was obtained by integrating their respective peak areas in their XPS spectra. Fig. 4c shows the Pd:Ni composition average of all samples after the indicated treatments. The results show that annealed and acid treated samples are composed of a Pd-rich surface, especially after acid treatment due to the effective removal of surface Ni in the form of oxide. HOR and ORR measurements of both annealed and acid treated samples result in a Ni enrichment of the surface. This provides evidence for the Ni diffusion to the surface triggered by its stronger OH^- adsorption energy compared to Pd [73]. After HOR measurements the averaged compositions result in almost equal amounts of superficial Pd:Ni (Table S2, Supporting Information). However, after ORR, annealed samples exhibit a much higher increase in surface Ni than ORR-measured acid treated samples, evincing the more hindered diffusion of Ni through a Pd overlayer.

Both Pd and Ni oxidated species were quantified from XPS deconvoluted spectra and averaged after every treatment as shown in Fig. 4d and Fig. 4e respectively. As shown, the higher metallic Pd on the surface is observed after both annealing and acid treatment, whereas oxidated Pd species (Pd^{2+} and Pd^{4+}) are formed during electrochemical testing. However, spectra of acid treated samples revealed PdO is still present. HOR measurements mainly result in the higher valence oxides, indicating the formation of Pd^{4+} species (PdO_2) from the oxidation of both Pd and, partially, PdO. ORR testing also leads to Pd oxidation, although the resulting alloys are primarily composed of a Pd^{2+} oxide. In contrast to Pd, Ni oxidated species are present already in the annealed samples due to the ease by which Ni oxidizes in air. Annealed samples show a major amount of $Ni(OH)_2$, which increases drastically after HOR and ORR measurements due to contact with the alkaline electrolyte. Acid treatment removes most of the Ni hydroxide, causing a rise of 30% in the relative amounts of both Ni and NiO. Since both Ni and NiO dissolves in acidic media and Ni forms a hydroxide in aqueous solutions [74], the remaining Ni and NiO is attributed to subsurface Ni that is not reachable by the electrolyte or the HCl. This supports the formation of a Pd overlayer due to Ni removal upon contact with acid. The amount of Ni $(OH)_2$ becomes again significant after ORR and HOR testing, suggesting the diffusion of Ni through the Pd layer owing to the higher affinity of Ni for OH^- [75].

3.2. HOR

Fig. 5a shows the cathodic scan of HOR polarization curves of the annealed PdNi thin films together with a pure Pd thin film as a reference. The polarization curve of pure Ni is not shown as the HOR activity of

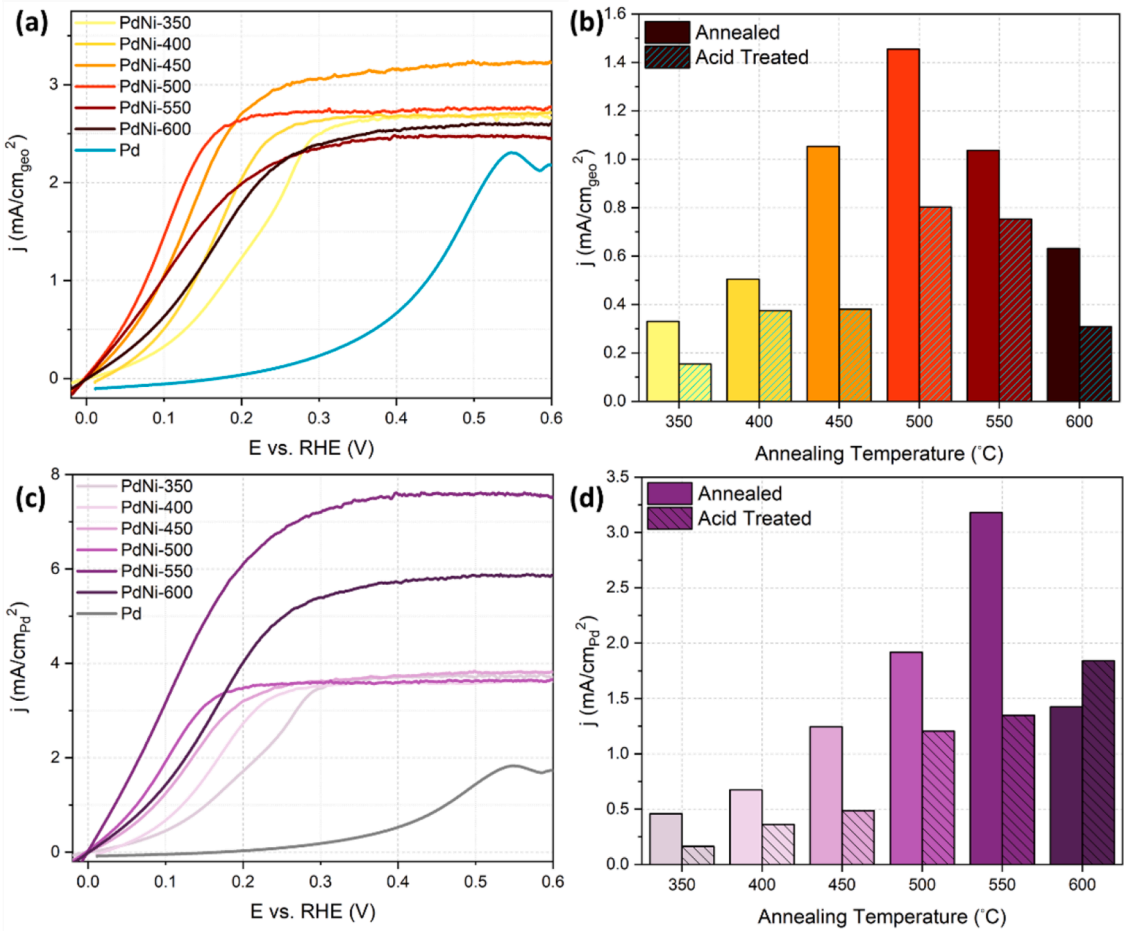

Fig. 5. HOR activity of PdNi samples and a pure Pd thin film in 0.1 M KOH: a) geometric currents of annealed samples at 1600 rpm, 50 mV/s; b) geometric activities of annealed and annealed + acid treated samples at 0.1 V; c) specific currents of annealed samples at 1600 rpm, 50 mV/s; d) specific activities of annealed and annealed + acid treated samples at 0.1 V.

pure Ni is more or less negligible [33]. With an onset potential at 0.17 V, the pure Pd film shows very low HOR activity, which is most likely due to a weaker HBE on Pd hydride that forms in H_2 atmosphere [76,77]. All annealed thin films show very low onset potentials, close to 0 V vs RHE, and exhibit slightly different potential responses as a result of the different Pd:Ni surface alloy compositions, as well as different limiting current densities possibly due to differences on the surface of the samples [78]. The HOR electroactivity exhibits slightly different potential responses, which are caused by slightly different Pd:Ni surface alloy compositions as a consequence of the different varying diffusion rates of Pd and Ni atoms throughout the film at the different annealing temperatures.

At 0.1 V, the geometric activities of annealed samples increase with increasing annealing temperature until 500 °C, after which they show a decay (Fig. 5b). Although the surface Pd% in Fig. 3b also follows a volcano-type trend, the rise and decline tendency in activity cannot be justified by the surface Pd. If the activity was dependent on the amount of Pd on the surface, PdNi-400 would have the highest activity since it has the largest Pd ECSA and higher surface roughness than PdNi-500. Instead, this trend at low overpotentials can be explained by both the degree of alloying and crystallite size. The degree of alloying in PdNi mixtures has been reported to increase up to 500 °C and remain almost constant thereafter [79–81]. Annealed thin film alloys typically exhibit the highest defect-mediated interdiffusion at annealing temperatures around 0.3 of the melting temperatures [82,83]. Thus, for Ni (1455 °C) and Pd (1555 °C) [84], 500 °C falls into the temperature range at which the highest atomic mixing through diffusion takes place, resulting in the largest degree of surface alloying. Similarly, the crystallite size increase with increasing annealing temperature might be the reason behind the activity decay after 500 °C [85–87], as well as grain agglomeration, which is not favorable for electrochemical reactions on bifunctional surfaces [85–88]. Thus, from the results presented above it is reasonable to infer that the rise and decay of the HOR geometric activity with increasing temperature demonstrates the relationship between Pd and Ni surface atomic distribution and the high HOR activity.

Specific activities (SA) expressed as current density per Pd ECSA (Fig. 5c) show that all PdNi alloys exhibit a higher activity than pure Pd, confirming the role of Ni in the enhancement of the HOR activity in alkaline media. Up to 500 °C, all samples reach the same limiting current density and they exhibit different half-wave potentials, which increase with increasing annealing temperature. The highest SA at 0.1 V vs. RHE (Fig. 5d) corresponds to the PdNi-550 sample, which shows the best utilization of surface Pd. This can be explained by the difference between the Pd ECSA before and after acid treatment shown in Fig. 3b, which suggests that PdNi-550 most likely has the highest Ni content at the very surface.

Acid treated annealed samples entirely composed of a Pd overlayer over the PdNi alloy were also evaluated in RDE. All annealed samples show a decrease in the geometric activity after acid treatment (Fig. 5b), which provides further evidence on the beneficial effect of the added oxophilicity provided by surface Ni. Similar to annealed samples, the resulting geometric activities reveal a volcano-type dependence on temperature. PdNi-500 shows the highest geometric activity at 0.1 V vs. RHE (0.80 mA/cm^2_{geo}), which is 5 times higher than that of PdNi-350, the sample with the lowest geometric activity at 0.1 V vs. RHE. The activity decrease after PdNi-500 is attributed to the steep decrease of the total surface area due to the effect of temperature on the surface roughness. The effect of decreasing total surface area with increasing temperature is further evidenced by the trend in SAs (Fig. 5d). The trend in activities in acid treated samples shows a better Pd utilization as annealing temperature increases, with PdNi-600 exhibiting the highest activity per Pd atom (1.84 mA/cm^2_{Pd}), most likely due to a much lower Pd ECSA evidenced by its CV (Fig. S4, Supporting Information). As previously shown in Fig. 3b, smoothening of the surface with increasing temperature also takes place at low annealing temperatures, although it shows a less prominent decrease. Thus, the increase in geometric activity between PdNi-350 and PdNi-500 cannot be explained by the surface smoothening effect. Instead, this increase in activity is ascribed to a ligand effect induced in the Pd overlayer by the Ni underneath that changes the d-band structure of the former [89,90]. The alteration of the Pd d-band is even more pronounced when $Ni(OH)_2$ species are present (i.e. even lower d-orbital occupancy). Furthermore, it has been reported that surface $Ni(OH)_2$ is beneficial for the HOR due to its oxophilicity that facilitates the bifunctional effect [41], so we consider the higher amount of $Ni(OH)_2$ during HOR measurements (Fig. 4d) also accountable for the HOR enhancement. The change in the electronic structure of Pd is further observed in the higher oxidation state of Pd during HOR (Fig. 4c). However, the modification of the Pd electronic properties can also be attributed to a lattice strain effect. This effect is also caused by the addition of Ni to the Pd lattice, which results in an alteration of the Pd-Pd bond distance and thus a modification of the electronic properties of the Pd overlayer [89,91]. The extent of both effects relies on the compositions of the underlying alloy, which result in different enhancements of the HOR activity.

Determination of the HBE is a good strategy to determine whether the enhancement of the HOR activity occurs through an electronic effect that modifies the HBE of Pd, or through a bifunctional effect where Ni $(OH)_2$ provides oxophilic sites for the OH^- adsorption. The HBE can be calculated experimentally from the hydrogen desorption peak on a metal surface by using the following equation [92,93]:

$$E_{M-H} = -FE_H - \frac{1}{2}TS^o \quad (4)$$

where E_{M-H} is the hydrogen binding energy, F is the Faraday's constant, E_H the hydrogen desorption peak potential, T is the temperature and S^o the entropy of H_2 at standard conditions. The H desorption peak potential can be obtained from the CV profiles of the annealed samples (Fig. S4, Supporting Information) between 0.25 and 0.35 V vs. RHE to calculate the HBE. All the annealed samples show H desorption peaks at lower potentials than pure Pd (0.48 V). The SA at 0.1 V vs. RHE was plotted against the HBE calculated from the H desorption peak (Fig. 6a, black fitted line). The plot shows a linear relationship between the SA and the HBE, with the activity increasing as the binding energy becomes weaker. This monotonic increase of the SA with decreasing HBE confirms that the latter is a crucial parameter for the HOR in alkaline electrolytes. Since it has been reported that the reason behind the sluggish HOR for Pd in alkaline media is the increase of the HBE with increasing pH [16,26], these results confirm that the weakening of the HBEs is crucial to enhance the HOR kinetics on Pd in alkaline conditions. Moreover, the fact that PdNi-550 shows the highest SA is in good agreement with DFT studies on the electronic structure of Pd-Ni systems, which affirmed that equal amounts of Ni and Pd result in the weakest HBE [94].

Electronic effects on the HOR activity are further evidenced by the linear relation between the SA of acid treated samples and the HBE (purple fitted line in Fig. 6a). Since all surfaces are entirely covered by Pd, the relation between the activity of acid treated samples and their HBE proves once again that the weaker HBE is undoubtedly responsible for the improved HOR kinetics in PdNi alloys. However, the lower slope in the fitted curve of acid treated samples shows that the activity increase with the weakening of the HBE is less pronounced in the absence of surface Ni. This also proves the favorable role of surface Ni in catalyzing the HOR reaction. As explained above, the weakening of the HBE is ascribed to lattice and electronic effects caused by the addition of Ni to the Pd lattice, which results in an alteration of the electronic properties of Pd and thus its HBE. However, at the same time, the significant decrease in HOR activities after the removal of surface Ni (Fig. 4d) authenticates the role of the bifunctional effect, i.e. the absence of oxophilic sites translates into a less pronounce enhancement of HOR kinetics.

Tafel analysis of the annealed samples revealed Tafel slopes between

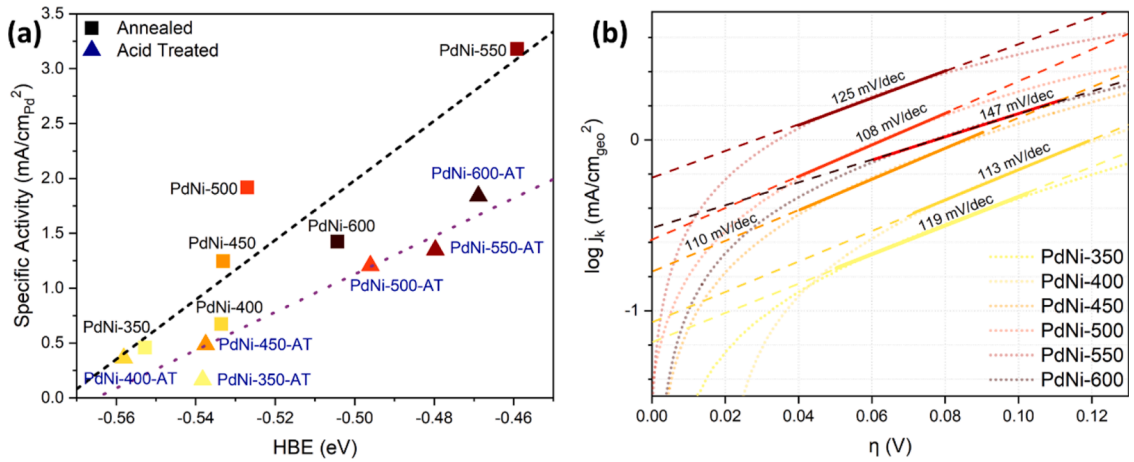

Fig. 6. (a) Specific activities of annealed and annealed + acid treated samples against the hydrogen binding energy and (b) Tafel plots and slopes of PdNi annealed samples.

108 and 147 mV/dec (Fig. 6b). The slopes follow the same volcano-type dependence with temperature as the geometric activities, with PdNi-500 showing the lowest slope and thus faster HOR kinetics. The intercepts of the Tafel plots were used to calculate the exchange current densities. When normalizing to the Pd ECSA, PdNi-550 showed the highest exchange current density among all annealed samples (1.85 mA/cm$^2_{Pd}$), which agrees with its SA at 0.1 V (Fig. 5d). The high Tafel slopes indicate that the charge transfer step (Heyrovsky or Volmer) is likely the rate determining step on all surfaces [18,90]. This is in good agreement with previous studies claiming that the HOR rate is controlled by the Volmer step on PGMs, where OH^- affects its rate merely through hindering the H adsorption rather than being an active participant in the surface reaction [95,96].

The results presented above provide evidence of the extensively

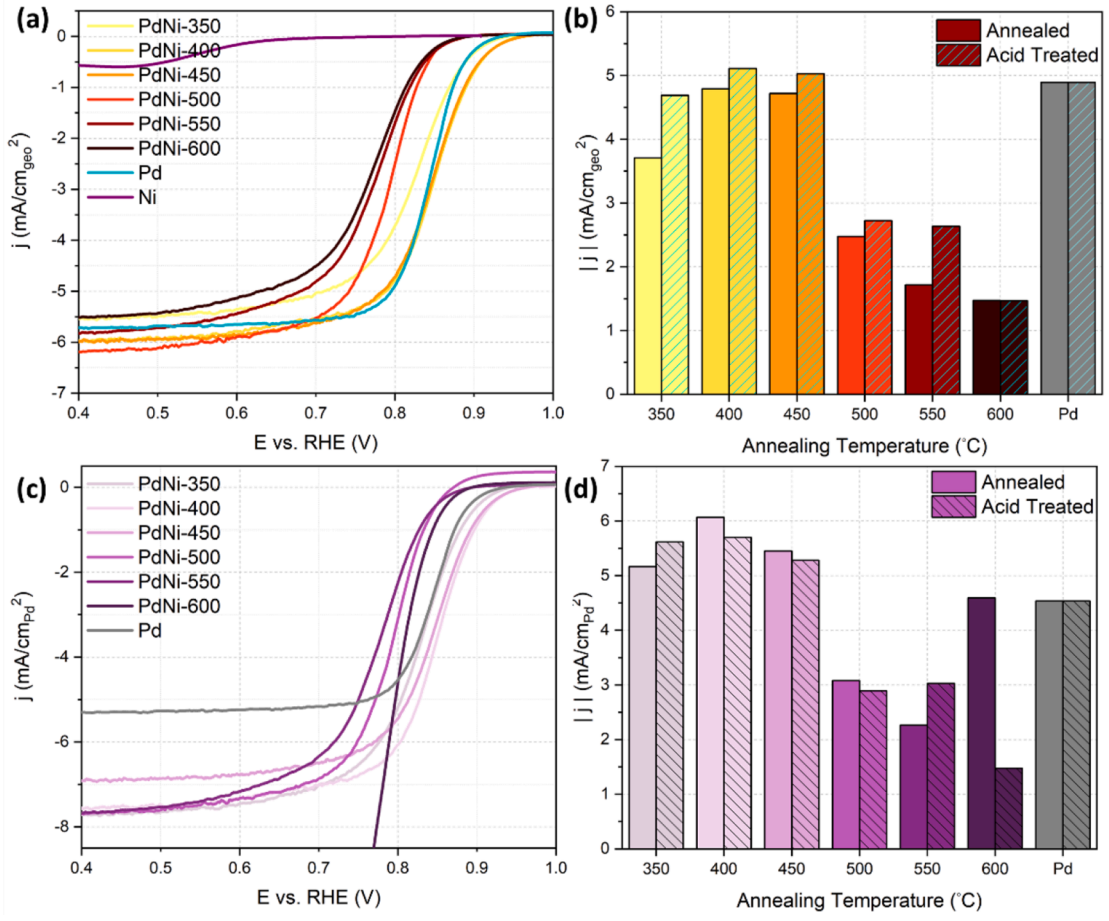

Fig. 7. ORR activity of PdNi samples and a pure Pd thin film in 0.1 M KOH: a) geometric currents of annealed samples at 1600 rpm, 50 mV/s; b) geometric activities of annealed and annealed + acid treated samples at 0.8 V; c) specific currents of annealed samples at 1600 rpm, 50 mV/s; d) specific activities of annealed and annealed + acid treated samples at 0.8 V. This potential has been chosen for comparing activities because at 0.8 V all samples were found at the kinetic and mass transport mixed region.

discussed role of Ni in improving the HOR kinetics in alkaline media. It has been broadly argued that the reason behind the increased HOR activity is lowering of the energy barrier of the Volmer step through added oxophilicity from surface Ni/Ni$(OH)_2$ atoms, which provides crucial adsorption sites for the OH^- adsorption [24,33,97]. However, we conclude that, although both the so-called bifunctional mechanism and the HBE are accountable for the enhanced HOR activity, the latter is the dominant descriptor of the HOR activity on Pd-based catalysts. In conclusion, the role of Ni in catalyzing the HOR comprises a major electronic effect that modifies the HBE of Pd and, to a lesser extent, a bifunctional effect through added oxophilicity. This is in good agreement with previous studies stating that in PGMs the reason for slower HOR kinetics is attributed to a stronger HBE in base, which affects both H and H_2O adsorption and thus the rate of the Volmer step [16,26,95,96].

3.3. ORR

Fig. 7a shows the cathodic scan of ORR polarization curves of the annealed PdNi thin films together with pure Ni and pure Pd thin films as reference. The curves show two different sets of onset potentials, with pure Pd and samples annealed at low temperatures (350 – 450 °C) showing the highest onset potential. Annealing at temperatures above 450 °C results in a significant decrease of the half-way potential, although they all exhibit very similar limiting current densities below 0.6 V vs RHE. PdNi-400 and PdNi-450 present the highest onset and half-wave potentials. The higher activities at low annealing temperatures seem to correlate well with the ratio of Pd surface area to subsurface Pd (Fig. 3b), with PdNi-400 and Pd-450 showing the largest amount of surface Pd per subsurface Pd. In other words, high amounts of surface Pd and subsurface Ni result in substantial ORR activities. This correlation is evidenced when comparing PdNi-400 and PdNi-500. As shown in Fig. 3b, these samples have very similar Pd surface areas (0.151 cm^2_{Pd} vs. 0.154 cm^2_{Pd}), although PdNi-400 has 5% more surface Ni derived from XPS measurements. The slightly higher surface Ni content in PdNi-400 is responsible for the 50 mV higher half-wave potential compared to PdNi-500, thereby corroborating the beneficial effect of subsurface Ni on the ORR. Thus, the significant decrease in activities above 450 °C is attributed to the major decrease in Ni beneath the PdNi surface layer (Fig. 3b). Whereas the presence of Ni underneath a Pd layer seems to result in higher activities, surface Ni seems to be disadvantageous for the ORR kinetics because there is no annealed sample performing remarkably better than Pd at any potential.

ORR specific activities of annealed samples also show a decrease in activities at annealing temperatures above 450 °C (Fig. 7c), most likely also attributed to Ni content in the top layers. However, when normalizing for the Pd surface area, PdNi-350, PdNi-400 and PdNi-450 show a better Pd utilization than pure Pd at 0.8 V vs. RHE (Fig. 7d). Again, the higher SAs follow the trend of higher surface Pd and higher subsurface Ni. All annealed samples reach higher limiting current densities than pure Pd, with PdNi-600 showing the largest limiting current due to a much lower Pd surface area.

The geometric activities of acid treated samples demonstrate a small increase in activity compared to the non-acid treated samples, with PdNi-350, PdNi-400 and PdNi-450 showing higher activities than Pd at 0.8 V (Fig. 7b). However, acid treated samples annealed at temperatures above 450 °C show ORR activities markedly lower than the rest, including Pd. Again, this is attributed to their lower subsurface Ni content (Fig. 3b). The reason behind the positive effect of subsurface Ni is ascribed to a d-orbital coupling effect between the two transition metals, which has been reported to result beneficial in bimetallic catalysts for the ORR in numerous studies [15,98–100]. The d-orbital coupling between the two metals results in a decrease of the Gibbs free energy of the electron transfer steps in the ORR, thereby enhancing the reaction by weakening the desorption of oxygenated intermediates on Pd [13,14]. Furthermore, the coupling effect is enhanced if Ni is found in the oxidized form (i.e. even lower d-orbital occupancy) so the presence of Ni$(OH)_2$ is also favorable for the ORR (Fig. 4d). Alloying with Ni/Ni$(OH)_2$ therefore results in a boosting of the ORR activity through an electronic effect that shifts downwards d-band center of Pd, which already exhibits a good O—O bond breakage. In the same way, since the kinetics of the O—O breakage on Ni is very slow, addition of Ni into a Pd lattice is beneficial only if the former is not present at the surface. Thus, the higher activity of PdNi-350-AT, PdNi-400-AT and PdNi-450-AT is assigned to a higher subsurface Ni content lowering the d-band center of the Pd layer above. The lower activity at higher temperatures is also attributed to a lower surface area owing to a higher surface smothering at those temperatures. However, their also low SAs (Fig. 7d) confirm that it is not attributable to a smoother surface. SAs provide even stronger evidence of the better Pd utilization in PdNi alloys compared to pure Pd.

The kinetics of the ORR were studied by collecting ORR polarization curves at different rotation speeds (Fig. S5, supporting information). The data was analyzed by extracting Koutecky-Levich (K-L) plots from the mass-transport region of the corresponding ORR polarization curves (i.e. 0.4 V). This potential was chosen to assure that all samples had the same contribution from kinetic and mass transport currents. The transferred electron number (n) was obtained using the K-L equation[101]:

$$\frac{1}{j} = \frac{1}{j_k} + \frac{1}{j_d} = \frac{1}{j_k} + \frac{1}{B\omega^{1/2}} \tag{5}$$

$$B = 0.2nF(D_{O_2})^{\frac{2}{3}}(\nu)^{-\frac{1}{6}}C_{O_2} \tag{6}$$

where j is the measured current density, j_k and j_d are the kinetic and diffusion-limited current densities, respectively, n is the number of electrons transfer per O_2 molecule, ω is the electrode rotation rate, F is the Faraday constant (96,485 C/mol), D_{O_2} is the diffusion coefficient of O_2 in KOH 0.1 M (1.9×10^{-5} cm^2/s), ν the kinetic viscosity (0.01 cm^2/s) and C_{O_2} is the bulk concentration of O_2 (1.2×10^{-6} mol/cm^3) [46, 102]. The constant 0.2 is used when the rotation rate is expressed in rpm.

Fig. 8a shows the K-L plots for ORR on the annealed samples. All samples studied present linear and parallel K-L lines, which indicate first order kinetics with respect to molecular oxygen [103]. The transferred electron number was calculated from the K-L slopes and it was found to be 4.3–4.5 for all annealed samples (Table S1, Supporting Information). The n values exceeded 4, which could be partly attributed to inherent errors associated with the partial fulfillment of the assumptions of the K-L analysis in the considered electrocatalytic system [101]. These values confirm that the ORR is governed by a 4-electron pathway, thereby reducing O_2 to OH^- during the reaction. A dominant 4-electron pathway was also observed in previous studies for Pd-based catalysts in alkaline conditions [46,104]. K-L analysis of acid treated samples (Fig. 8b) also exhibit parallel and linear plots, but much more similar intercepts indicating very similar kinetic current densities (j_k). The n value was also found to be around 4 for all acid treated samples, indicating the same reduction pathway as annealed samples.

The results presented in this section support the picture of a beneficial effect of alloying PGMs with transition metals with lower d-orbital occupancy to enhance the ORR kinetics, which has been discussed in earlier studies. The overall increase in the ORR activity when surface Ni is removed by acid treatment evidences the ineffectiveness of Ni as a direct active site in this reaction. However, the activities of acid treated samples surpassing the activity of pure Pd justify the electronic effect induced by the Ni underneath. Hence, we confirm the positive effect of lowering the d-band center of transition metals with excellent O—O breakage and unfavorable desorption of oxygenated species.

4. Conclusions

In this study, we investigated how electronic and bifunctional effects in alloyed PdNi thin films and in a Pd layer over a PdNi alloy influence

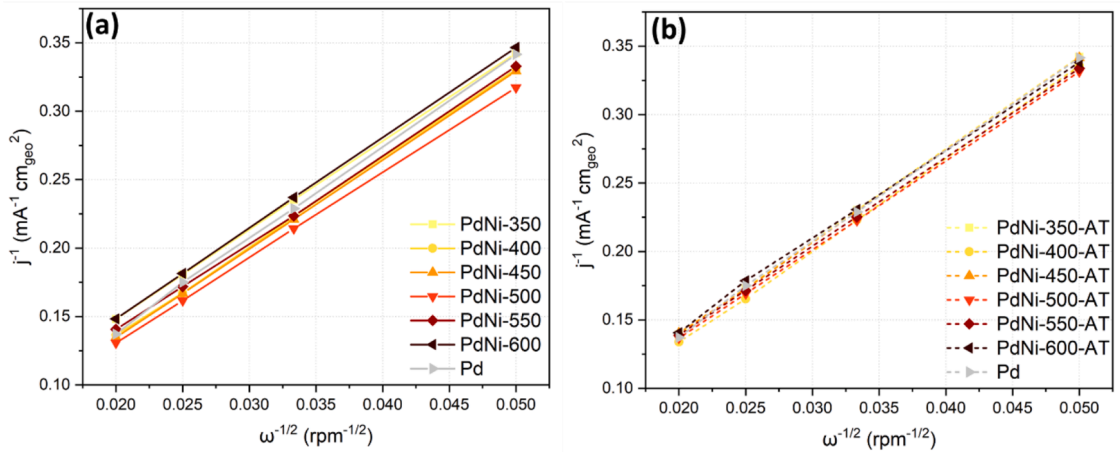

Fig. 8. K-L plots derived from the ORR polarization curves at 0.4 V of (a) annealed samples and (b) acid treated samples.

both HOR and ORR activities in alkaline media. HOR measurements revealed that both electronic and bifunctional effects play a role in accelerating the HOR kinetics. It was found that the main responsible for the activity enhancement observed in PdNi alloys is the weaker HBE of Pd as a result of the Ni addition. Removal of surface Ni by acid treatment resulted in an overall decrease of the HOR activities, thereby providing strong evidence that surface $Ni/Ni(OH)_2$ is also boosting the HOR kinetics by providing oxophilic sites for OH^- adsorption, i.e. a bifunctional mechanism. ORR measurements also displayed a beneficial effect of alloying Pd with Ni. In contrast to the HOR, surface Ni has a detrimental effect on the ORR kinetics in alkaline media, as evinced by the overall activity increase after forming a Pd overlayer by acid treatment. The resulting protective Pd layer turned out to be a slightly more effectual ORR catalyst due to electronic effects that favor the desorption of oxygenated species and thus the ORR kinetics. Therefore, we confirm that structural effects are crucial if the electronic effects are meant to be distinguished, which in turn are the main reason for the observed HOR and ORR activity enhancement in alkaline media.

Credit author statement

Both authors designed the electrochemical experiments. G.M.S. performed all fabrication and experiments. G.M.S. wrote the first draft and both authors edited the paper. Both authors discussed the results, read and approved the final version of the paper.

Declaration of Competing Interest

The authors declare that they have no known competing financial interests or personal relationships that could have appeared to influence the work reported in this paper.

Acknowledgments

This project is financially supported by the Swedish Foundation for Strategic Research (Project No. EM16-0060) and the Swedish Research Council (Project No. 2018-03927). Sample fabrication was performed in part at Myfab clean room at Chalmers. We also thank Chalmers Materials Analysis Laboratory (CMAL) for part of the physical characterization.

Supplementary materials

Supplementary material associated with this article can be found, in the online version, at doi:10.1016/j.electacta.2022.140425.

References

[1] R. Borup, et al., Scientific aspects of polymer electrolyte fuel cell durability and degradation, Chem. Rev. 107 (2007) 3904–3951.
[2] U. Eberle, B. Müller, R. Von Helmolt, Fuel cell electric vehicles and hydrogen infrastructure: status 2012, Energy Environ. Sci. 5 (2012) 8780–8798.
[3] M. Kiani, et al., Recent developments in electrocatalysts and future prospects for oxygen reduction reaction in polymer electrolyte membrane fuel cells, J. Energy Chem. 27 (2018) 1124–1139.
[4] S. Shahgaldi, J. Hamelin, Improved carbon nanostructures as a novel catalyst support in the cathode side of PEMFC: a critical review, Carbon N. Y. 94 (2015) 705–728.
[5] I.E.L. Stephens, A.S. Bondarenko, U. Grønbjerg, J. Rossmeisl, I Chorkendorff, Understanding the electrocatalysis of oxygen reduction on platinum and its alloys, Energy Environ. Sci. 5 (2012) 6744–6762.
[6] A. Rabis, P. Rodriguez, T.J. Schmidt, Electrocatalysis for polymer electrolyte fuel cells: recent achievements and future challenges, ACS Catal. 2 (2012) 864–890.
[7] T. Abdel-Baset, et al., U.S. Department of Energy Hydrogen and Fuel Cell Technology Office. 2019 Annual Merit Review and Peer Evaluation Report., 2020, pp. 1–711. https://energy.gov/eere/fuelcells/doe-technical-targets-polymer-electrolyte-membrane-fuel-cell-components, https://doi.org/10.2172/1220127.
[8] Q. He, E.J Cairns, Review-recent progress in electrocatalysts for oxygen reduction suitable for alkaline anion exchange membrane fuel cells, J. Electrochem. Soc. 162 (2015) F1504–F1539.
[9] Z.F. Pan, L. An, T.S. Zhao, Z.K Tang, Advances and challenges in alkaline anion exchange membrane fuel cells, Prog. Energy Combust. Sci. 66 (2018) 141–175.
[10] J.R. Varcoe, R.C.T. Slade, G.L. Wright, Y. Chen, Steady-state dc and impedance investigations of H_2/O_2 alkaline membrane fuel cells with commercial Pt/C, Ag/C, and Au/C cathodes, J. Phys. Chem. B 110 (2006) 21041–21049.
[11] G.F. McLean, T. Niet, S. Prince-Richard, N. D, An assessment of AFC technology, Int. J. Hydrog. Energy 27 (2002) 507–526.
[12] I.E.L. Stephens, et al., Tuning the activity of Pt(111) for oxygen electroreduction by subsurface alloying, J. Am. Chem. Soc. 133 (2011) 5485–5491.
[13] Y. Wang, P.B Balbuena, Design of oxygen reduction bimetallic catalysts: ab-initio-derived thermodynamic guidelines, J. Phys. Chem. B 109 (2005) 18902–18906.
[14] F.H.B. Lima, et al., Catalytic activity - D-band center correlation for the O_2 reduction reaction on platinum in alkaline solutions, J. Phys. Chem. C 111 (2007) 404–410.
[15] S.A. Park, H. Lim, Y.T. Kim, Enhanced oxygen reduction reaction activity due to electronic effects between Ag and Mn_3O_4 in alkaline media, ACS Catal. 5 (2015) 3995–4002.
[16] J. Durst, et al., New insights into the electrochemical hydrogen oxidation and evolution reaction mechanism, Energy Environ. Sci. 7 (2014) 2255–2260.
[17] R. Jervis, et al., Hydrogen oxidation on PdIr/C catalysts in alkaline media, J. Electrochem. Soc. 161 (2014) F458–F463.
[18] Y. Cong, B. Yi, Y. Song, Hydrogen oxidation reaction in alkaline media: from mechanism to recent electrocatalysts, Nano Energy 44 (2018) 288–303.
[19] T.J. Schmidt, V. Stamenkovic, P.N. Ross, N.M. Markovic, Temperature dependent surface electrochemistry on Pt single crystals in alkaline electrolyte: part 3. The oxygen reduction reaction, Phys. Chem. Chem. Phys. 5 (2003) 400–406.
[20] Y. Wang, et al., Pt-Ru catalyzed hydrogen oxidation in alkaline media: oxophilic effect or electronic effect? Energy Environ. Sci. 8 (2015) 177–181.
[21] W. Sheng, H.A. Gasteiger, Y. Shao-Horn, Hydrogen oxidation and evolution reaction kinetics on platinum: acid vs alkaline electrolytes, J. Electrochem. Soc. 157 (2010) B1529.
[22] J. Li, et al., Experimental proof of the bifunctional mechanism for the hydrogen oxidation in alkaline media, Angew. Chem. 129 (2017) 15800–15804.

[23] M. Alesker, et al., Palladium/nickel bifunctional electrocatalyst for hydrogen oxidation reaction in alkaline membrane fuel cell, J. Power Sources 304 (2016) 332–339.
[24] M. Shviro, S. Polani, R.E. Dunin-Borkowski, D. Zitoun, Bifunctional electrocatalysis on Pd-Ni core–shell nanoparticles for hydrogen oxidation reaction in alkaline medium, Adv. Mater. Interfaces 5 (2018) 1–8.
[25] S. Lu, Z Zhuang, Investigating the influences of the adsorbed species on catalytic activity for hydrogen oxidation reaction in alkaline electrolyte, J. Am. Chem. Soc. 139 (2017) 5156–5163.
[26] W. Sheng, et al., Correlating hydrogen oxidation and evolution activity on platinum at different pH with measured hydrogen binding energy, Nat. Commun. 6 (2015) 6–11.
[27] J. Ohyama, D. Kumada, A. Satsuma, Improved hydrogen oxidation reaction under alkaline conditions by ruthenium-iridium alloyed nanoparticles, J. Mater. Chem. A 4 (2016) 15980–15985.
[28] W. Sheng, et al., Non-precious metal electrocatalysts with high activity for hydrogen oxidation reaction in alkaline electrolytes, Energy Environ. Sci. 7 (2014) 1719–1724.
[29] R. Pattabiraman, Electrochemical investigations on carbon supported palladium catalysts, Appl. Catal. A Gen. 153 (1997) 9–20.
[30] H. Erikson, A. Sarapuu, J. Solla-Gullón, K Tammeveski, Recent progress in oxygen reduction electrocatalysis on Pd-based catalysts, J. Electroanal. Chem. 780 (2016) 327–336.
[31] M. Shao, Palladium-based electrocatalysts for hydrogen oxidation and oxygen reduction reactions, J. Power Sources 196 (2011) 2433–2444.
[32] M.H. Martin, A. Lasia, Study of the hydrogen absorption in Pd in alkaline solution, Electrochim. Acta 53 (2008) 6317–6322.
[33] M. Alesker, et al., Palladium/nickel bifunctional electrocatalyst for hydrogen oxidation reaction in alkaline membrane fuel cell, J. Power Sources 304 (2016) 332–339.
[34] B. Li, J Prakash, Oxygen reduction reaction on carbon supported palladium-nickel alloys in alkaline media, Electrochem. Commun. 11 (2009) 1162–1165.
[35] L. Chen, et al., Nanoporous PdNi bimetallic catalyst with enhanced electrocatalytic performances for electro-oxidation and oxygen reduction reactions, Adv. Funct. Mater. 21 (2011) 4364–4370.
[36] S. Jiang, B. Yi, Q. Zhao, H. Yu, Z Shao, Palladium-nickel catalysts based on ordered titanium dioxide nanorod arrays with high catalytic peformance for formic acid electro-oxidation, RSC Adv. 7 (2017) 11719–11723.
[37] J.A.D Del Rosario, et al., Enhancing role of nickel in the nickel-palladium bilayer for electrocatalytic oxidation of ethanol in alkaline media, J. Phys. Chem. C 118 (2014) 22473–22478.
[38] L. Zhang, Q. Chang, H. Chen, M. Shao, Recent advances in palladium-based electrocatalysts for fuel cell reactions and hydrogen evolution reaction, Nano Energy 29 (2016) 198–219.
[39] N. Ramaswamy, et al., Hydrogen oxidation reaction in alkaline media: relationship between electrocatalysis and electrochemical double-layer structure, Nano Energy 41 (2017) 765–771.
[40] Z. Zhou, Y. Liu, J. Zhang, H. Pang, G Zhu, Non-precious nickel-based catalysts for hydrogen oxidation reaction in alkaline electrolyte, Electrochem. Commun. 121 (2020), 106871.
[41] Y. Pan, G. Hu, J. Lu, L. Xiao, L. Zhuang, $Ni(OH)_2$-Ni/C for hydrogen oxidation reaction in alkaline media, J. Energy Chem. 29 (2019) 111–115.
[42] A.G. Oshchepkov, A. Bonnefont, E.R. Savinova, On the influence of the extent of oxidation on the kinetics of the hydrogen electrode reactions on polycrystalline nickel, Electrocatalysis 11 (2020) 133–142.
[43] L. Sun, et al., Ternary PdNi-based nanocrystals supported on nitrogen-doped reduced graphene oxide as highly active electrocatalysts for the oxygen reduction reaction, Electrochim. Acta 235 (2017) 543–552.
[44] X. Ren, et al., PdNi alloy decorated 3D hierarchically N, S co-doped macro-mesoporous carbon composites as efficient free-standing and binder-free catalysts for Li-O_2 batteries, J. Mater. Chem. A 6 (2018) 10856–10867.
[45] Y. Li, et al., One-step rapid in-situ synthesis of nitrogen and sulfur co-doped three-dimensional honeycomb-ordered carbon supported PdNi nanoparticles as efficient electrocatalyst for oxygen reduction reaction in alkaline solution, Electrochim. Acta 253 (2017) 445–454.
[46] M. Wang, et al., PdNi hollow nanoparticles for improved electrocatalytic oxygen reduction in alkaline environments, ACS Appl. Mater. Interfaces 5 (2013) 12708–12715.
[47] P.J. Rheinländer, J. Herranz, J. Durst, H.A Gasteiger, Kinetics of the hydrogen oxidation/evolution reaction on polycrystalline platinum in alkaline electrolyte reaction order with respect to hydrogen pressure, J. Electrochem. Soc. 161 (2014) F1448–F1457.
[48] L. Zhao, et al., Mechanistic Insights into the hydrogen oxidation reaction on PtNi alloys in alkaline media: a first-principles investigation, ACS Appl. Mater. Interfaces 12 (2020) 40248–40260.
[49] N. Ramaswamy, S Mukerjee, Influence of inner- and outer-sphere electron transfer mechanisms during electrocatalysis of oxygen reduction in alkaline media, J. Phys. Chem. C 115 (2011) 18015–18026.
[50] X. Ge, et al., Oxygen reduction in alkaline media: from mechanisms to recent advances of catalysts, ACS Catal. 5 (2015) 4643–4667.
[51] M. Schalenbach, et al., The electrochemical dissolution of noble metals in alkaline media, Electrocatalysis 9 (2018) 153–161.
[52] A. Zadick, L. Dubau, N. Sergent, G. Berthomé, M Chatenet, Huge instability of Pt/C catalysts in alkaline medium, ACS Catal. 5 (2015) 4819–4824.
[53] C. Lafforgue, A. Zadick, L. Dubau, F. Maillard, M. Chatenet, Selected review of the degradation of Pt and Pd-based carbon-supported electrocatalysts for alkaline fuel cells: towards mechanisms of degradation, Fuel Cells 18 (2018) 229–238.
[54] C. Wei, et al., Recommended practices and benchmark activity for hydrogen and oxygen electrocatalysis in water splitting and fuel cells, Adv. Mater. 31 (2019) 1–24.
[55] H.A. Gasteiger, S.S. Kocha, B. Sompalli, F.T. Wagner, Activity benchmarks and requirements for Pt, Pt-alloy, and non-Pt oxygen reduction catalysts for PEMFCs, Appl. Catal. B Environ. 56 (2005) 9–35.
[56] V. Ćolić, et al., Experimental aspects in benchmarking of the electrocatalytic activity, ChemElectroChem 2 (2015) 143–149.
[57] J.C. Myland, K.B Oldham, Uncompensated resistance. 1. The effect of cell geometry, Anal. Chem. 72 (2000) 3972–3980.
[58] V.S. Smentkowski, Trends in sputtering, Prog. Surf. Sci. 64 (2000) 1–58.
[59] H.L. Skriver, N.M Rosengaard, Surface energy and work function of elemental metals, Phys. Rev. B 46 (1992) 7157–7168.
[60] J. Greeley, M Mavrikakis, Surface and subsurface hydrogen: adsorption properties on transition metals and near-surface alloys, J. Phys. Chem. B 109 (2005) 3460–3471.
[61] M. Grdeń, A. Czerwiński, EQCM studies on Pd-Ni alloy oxidation in basic solution, J. Solid State Electrochem. 12 (2008) 375–385.
[62] Z.X. Liang, T.S. Zhao, J.B. Xu, L.D. Zhu, Mechanism study of the ethanol oxidation reaction on palladium in alkaline media, Electrochim. Acta 54 (2009) 2203–2208.
[63] R. Liang, A. Hu, J. Persic, Y. Norman Zhou, Palladium nanoparticles loaded on carbon modified TiO_2 nanobelts for enhanced methanol electrooxidation, *Nano Micro Lett.* 5 (2013) 202–212.
[64] D.S. Hall, C. Bock, B.R. MacDougall, The electrochemistry of metallic nickel: oxides, hydroxides, hydrides and alkaline hydrogen evolution, J. Electrochem. Soc. 160 (2013) F235–F243.
[65] M. Alsabet, M. Grdeń, G. Jerkiewicz, Electrochemical growth of surface oxides on nickel. Part 3: formation of β-NiOOH in relation to the polarization potential, polarization time, and temperature, Electrocatalysis 6 (2014) 60–71.
[66] Y. Suo, L. Zhuang, J Lu, First-principles considerations in the design of Pd-alloy catalysts for oxygen reduction, Angew. Chem. Int. Ed. 46 (2007) 2862–2864.
[67] S. Henning, J. Herranz, H.A Gasteiger, Bulk-palladium and palladium-on-gold electrocatalysts for the oxidation of hydrogen in alkaline electrolyte, J. Electrochem. Soc. 162 (2015) F178–F189.
[68] D.A.J. Rand, R. Woods, The nature of adsorbed oxygen on rhodium, palladium and gold electrodes, J. Electroanal. Chem. 31 (1971) 29–38.
[69] Z. Yang, Y. Ling, Y. Zhang, G Xu, High performance palladium supported on nanoporous carbon under anhydrous condition, Sci. Rep. 6 (2016) 1–10.
[70] W. He, et al., 3D β-$Ni(OH)_2$ nanowires/RGO composite prepared by phase transformation method for superior electrochemical performance, Sci. Rep. 9 (2019) 1–8.
[71] M.C. Biesinger, B.P. Payne, L.W.M. Lau, A. Gerson, R.S.C. Smart, X-ray photoelectron spectroscopic chemical state quantification of mixed nickel metal, oxide and hydroxide systems, Surf. Interface Anal. 41 (2009) 324–332.
[72] X. Yu, et al., Hydrogen evolution reaction in alkaline media: alpha- or beta-nickel hydroxide on the surface of platinum? ACS Energy Lett. 3 (2018) 237–244.
[73] J.K. Nørskov, et al., Origin of the overpotential for oxygen reduction at a fuel-cell cathode, J. Phys. Chem. B 108 (2004) 17886–17892.
[74] S.E. Ziemniak, M.E. Jones, K.E.S Combs, Solubility and phase behavior of Nickel Oxide in aqueous sodium phosphate solutions at elevated temperatures, J. Solut. Chem. 21 (1992) 1153–1176.
[75] X. Lu, M. Ahmadi, F.J. Disalvo, H.D. Abruña, Enhancing the electrocatalytic activity of Pd/M (M = Ni, Mn) nanoparticles for the oxygen reduction reaction in alkaline media through electrochemical dealloying, ACS Catal. 10 (2020) 5891–5898.
[76] M. Johansson, et al., Hydrogen adsorption on palladium and palladium hydride at 1bar, Surf. Sci. 604 (2010) 718–729.
[77] R. Griessen, N. Strohfeldt, H Giessen, Thermodynamics of the hybrid interaction of hydrogen with palladium nanoparticles, Nat. Mater. 15 (2016) 311–317.
[78] Y. Qian, P. Du, P. Wu, C. Cai, D.F Gervasio, Chemical nature of catalytic active sites for the oxygen reduction reaction on nitrogen-doped carbon-supported non-noble metal catalysts, J. Phys. Chem. C 120 (2016) 9884–9896.
[79] W. Wang, et al., Carbon-supported Pd-Co bimetallic nanoparticles as electrocatalysts for the oxygen reduction reaction, J. Power Sources 167 (2007) 243–249.
[80] H. Liu, A. Manthiram, Tuning the electrocatalytic activity and durability of low cost Pd70Co30 nanoalloy for oxygen reduction reaction in fuel cells, Electrochem. Commun. 10 (2008) 740–744.
[81] D.S. Choi, A.W. Robertson, J.H. Warner, S.O. Kim, H Kim, Low-temperature chemical vapor deposition synthesis of Pt–Co alloyed nanoparticles with enhanced oxygen reduction reaction catalysis, Adv. Mater. 28 (2016) 7115–7122.
[82] D. Gupta, Special aspects of diffusion in metallic thin films, Mater. Res. Soc. Symp. Proc. 47 (1985) 11–26.
[83] L. Hultman, Thermal stability of nitride thin films, Vacuum 57 (2000) 1–30.
[84] E.H. TRIPP, Materials handbook, Nature 150 (1942).
[85] S. Benramache, B. Benhaoua, Influence of annealing temperature on structural and optical properties of ZnO: in thin films prepared by ultrasonic spray technique, Superlattices Microstruct. 52 (2012) 1062–1070.
[86] H. Metin, R. Esen, Annealing studies on CBD grown CdS thin films, J. Cryst. Growth 258 (2003) 141–148.

[87] K. Sugawara, Y. Minamide, M. Kawamura, Y. Abe, K. Sasaki, Agglomeration behavior of Ag films suppressed by alloying with some elements, Vacuum 83 (2008) 610–613.
[88] Y. She, Z. Lu, W. Fan, S. Jewell, M.K.H Leung, Facile preparation of PdNi/rGO and its electrocatalytic performance towards formic acid oxidation, J. Mater. Chem. A 2 (2014) 3894–3898.
[89] M.E. Scofield, et al., Role of chemical composition in the enhanced catalytic activity of Pt-based alloyed ultrathin nanowires for the hydrogen oxidation reaction under alkaline conditions, ACS Catal. 6 (2016) 3895–3908.
[90] J. Hu, K.A. Kuttiyiel, K. Sasaki, C. Zhang, R.R Adzic, Determination of hydrogen oxidation reaction mechanism based on Pt−H ad energetics in alkaline electrolyte, J. Electrochem. Soc. 165 (2018) J3355–J3362.
[91] X. Wang, et al., Strain effect in bimetallic electrocatalysts on the hydrogen evolution reaction, ACS Energy Lett. 3 (2018) 1198–1204.
[92] T. Bhowmik, M.K. Kundu, S Barman, Palladium nanoparticle-graphitic carbon nitride porous synergistic catalyst for hydrogen evolution/oxidation reactions over a broad range of pH and correlation of its catalytic activity with measured hydrogen binding energy, ACS Catal. 6 (2016) 1929–1941.
[93] G.S. Karlberg, et al., Cyclic voltammograms for H on Pt(111) and Pt(100) from first principles, Phys. Rev. Lett. 99 (2007) 1–4.
[94] L. Leppert, R. Kempe, S. Kümmel, Hydrogen binding energies and electronic structure of Ni-Pd particles: a clue to their special catalytic properties, Phys. Chem. Chem. Phys. 17 (2015) 26140–26148.
[95] J. Huang, P. Li, S Chen, Quantitative understanding of the sluggish kinetics of hydrogen reactions in alkaline media based on a microscopic hamiltonian model for the Volmer step, J. Phys. Chem. C 123 (2019) 17325–17334.
[96] S. Intikhab, J.D. Snyder, M.H Tang, Adsorbed hydroxide does not participate in the Volmer step of alkaline hydrogen electrocatalysis, ACS Catal. 7 (2017) 8314–8319.
[97] G. Shi, H. Yano, D.A. Tryk, A. Iiyama, H. Uchida, Highly active, CO-tolerant, and robust hydrogen anode catalysts: pt-M (M = Fe, Co, Ni) alloys with stabilized Pt-skin layers, ACS Catal. 7 (2017) 267–274.
[98] C. Xu, Y. Liu, Q. Hao, H. Duan, Nanoporous PdNi alloys as highly active and methanol-tolerant electrocatalysts towards oxygen reduction reaction, J. Mater. Chem. A 1 (2013) 13542–13548.
[99] M. Aguirre, C. del, B.L. Rivas, L.M. Fabietti, S.E Urreta, Enhanced performance of nano-electrocatalysts of Pd and PdCo in neutral and alkaline media, J. Appl. Electrochem. 49 (2019) 1–15.
[100] J. Kim, J.E. Park, T. Momma, T. Osaka, Synthesis of Pd-Sn nanoparticles by ultrasonic irradiation and their electrocatalytic activity for oxygen reduction, Electrochim. Acta 54 (2009) 3412–3418.
[101] R. Zhou, Y. Zheng, M. Jaroniec, S.Z. Qiao, Determination of the electron transfer number for the oxygen reduction reaction: from theory to experiment, ACS Catal. 6 (2016) 4720–4728.
[102] N.R. Elezović, B.M. Babić, L.J.M. Vračar, N.V. Krstajić, Oxygen reduction at platinum nanoparticles supported on carbon cryogel in alkaline solution, J. Serbian Chem. Soc. 72 (2007) 699–708.
[103] S. Mukerjee, S Srinivasan, Enhanced electrocatalysis of oxygen reduction on platinum alloys in proton exchange membrane fuel cells, J. Electroanal. Chem. 357 (1993) 201–224.
[104] N. Alexeyeva, et al., Electroreduction of oxygen on Vulcan carbon supported Pd nanoparticles and Pd-M nanoalloys in acid and alkaline solutions, Electrochim. Acta 56 (2011) 6702–6708.